Mon. Not. R. Astron. Soc. **372,** 151–162 (2006) doi:10.1111/j.1365-2966.2006.10834.x

First science with the Southern African Large Telescope: peering at the accreting polar caps of the eclipsing polar SDSS J015543.40+002807.2

D. O'Donoghue,[1⋆] D. A. H. Buckley,[1,2] L. A. Balona,[1] D. Bester,[2] L. Botha,[1] J. Brink,[1,2] D. B. Carter,[1] P. A. Charles,[1] A. Christians,[1] F. Ebrahim,[1,2] R. Emmerich,[1,2] W. Esterhuyse,[2] G. P. Evans,[1] C. Fourie,[1] P. Fourie,[1] H. Gajjar,[1,2] M. Gordon,[1] C. Gumede,[2] M. de Kock,[2] A. Koeslag,[2] W. P. Koorts,[1] H. Kriel,[1] F. Marang,[1] J. G. Meiring,[2] J. W. Menzies,[1] P. Menzies,[1] D. Metcalfe,[1] B. Meyer,[1] L. Nel,[2] J. O'Connor,[1] F. Osman,[1] C. du Plessis,[1] H. Rall,[1] A. Riddick,[1] E. Romero-Colmenero,[1] S. B. Potter,[1] C. Sass,[1] H. Schalekamp,[2] N. Sessions,[2] S. Siyengo,[1] V. Sopela,[1] H. Steyn,[1] J. Stoffels,[1] J. Scholtz,[1] G. Swart,[2] A. Swat,[2] J. Swiegers,[2] T. Tiheli,[1] P. Vaisanen,[1] W. Whittaker[2] and F. van Wyk[1]

[1]*South African Astronomical Observatory, Observatory, 7935 Cape Town, South Africa*
[2]*Southern African Large Telescope Foundation, Observatory, 7935 Cape Town, South Africa*

Accepted 2006 July 7. Received 2006 June 2; in original form 2005 November 25

ABSTRACT

We describe briefly the properties of the recently completed Southern African Large Telescope (SALT), along with its first light imager SALTICAM. Using this instrument, we present 4.3 h of high-speed unfiltered photometric observations of the eclipsing polar SDSS J015543.40+002807.2 with time-resolution as short as 112 ms, the highest-quality observations of this kind of any polar to date. The system was observed during its high-luminosity state. Two accreting poles are clearly seen in the eclipse light curve. The binary system parameters have been constrained: the white dwarf mass is at the low end of the range expected for cataclysmic variables. Correlations between the positions of the accretion regions on or near the surface of the white dwarf and the binary system parameters were established. The sizes of the accretion regions and their relative movement from eclipse to eclipse were estimated: they are typically 4°–7° depending on the mass of the white dwarf. The potential of these observations will only fully be realized when low-state data of the same kind are obtained and the contact phases of the eclipse of the white dwarf are measured.

Key words: accretion, accretion discs – binaries: close – novae, cataclysmic variables – X-rays: stars.

1 INTRODUCTION TO THE SOUTHERN AFRICAN LARGE TELESCOPE

The Southern African Large Telescope, colloquially known by its acronym SALT, has recently been completed. It is now in the final stages of commissioning and first stages of science operations. This paper describes the properties of the telescope and its imaging camera SALTICAM. It then presents the first science observations of an eclipsing magnetic cataclysmic variable (CV), SDSS J015543.40+002807.2, analyses the data and shows how our knowledge of this star has been advanced.

⋆E-mail: dod@saao.ac.za

Although the SALT has been described in the proceedings of SPIE conferences (e.g. Stobie, Meiring & Buckley 2000; Meiring et al. 2003; Meiring & Buckley 2004), these publications are not available in all astronomical libraries and not accessible on the Internet. Thus, a brief description of the SALT is appropriate. Its basic principle of operation is similar to that of the Arecibo radio telescope, employing a spherical primary mirror and a payload carrying the instrumentation which tracks the spherically shaped focal surface. This surface is concentric with the primary mirror and located at a distance of 13.08 m (half the radius of curvature) from the primary mirror. The overall optical design of the SALT is described in Swat et al. (2003).

The primary mirror is tilted so that its axis of symmetry is fixed at an inclination of 37° to the zenith. The telescope can move in

azimuth, but not in elevation, so it can observe any celestial object which reaches an altitude of 53°. The tracking capability described below extends this range of altitudes from 47° to 59°.

The basic concept for this telescope was proposed by Ramsey & Weedman (1984) and its first implementation was the construction of the Hobby–Eberly Telescope (HET) at McDonald Observatory. The SALT is the second such telescope and started off its development process using the design of the HET. However, many aspects of this design were improved on.

1.1 Primary mirror

The primary mirror is comprised of 91 hexagonal spherical segments 1 m across, 50 mm thick, and made of Astro-Sitall (Swiegers & Gajjar 2004). The arrangement of the primary segments is also hexagonal such that a circle of diameter 11 m would pass through the vertices of the hexagon. The individual segments are shaped to a global radius of curvature of the primary of 26.165 ± 0.0005 m, and figured to better than 1/15th wave rms. Each segment is supported on a mirror mount with nine points of support; three actuators move the segment in tip/tilt and piston. The mirror mounts are 'plugged' in to a steel space-frame truss which itself is kinematically supported on the telescope structure.

An alignment of the mirror segments with respect to each other to an accuracy of 0.06-arcsec rms takes place in the evening twilight and is achieved using a Shack–Hartmann wavefront camera, located at the centre of curvature of the primary mirror in a tower alongside the telescope building. The alignment is maintained using a system of capacitive edge sensors which are bonded to the six sides of each mirror segment, generating tiny but detectable changes in capacitance as the segments move with respect to each other during the night. These signals are fed to a closed-loop control system which adjusts the segment positioning every 20 s to maintain the original alignment of the mirror.

1.2 Tracker and payload

The payload at the prime focus is positioned using a 'Tracker' which is capable of movement in x, y, z, tip, tilt and rotation with accuracies of $\sim$5 μm and 1 arcsec (despite carrying a weight of more than a metric ton!). Tracking celestial objects requires adjustment of x and y, along with concomitant changes in tip and tilt. The focus of the telescope is controlled by a movement in z. The payload is also rotated about the telescope optical axis during observation to remove field rotation at the focal plane.

The payload includes a four-mirror spherical aberration corrector (SAC) (O'Donoghue 2000) to correct the huge spherical aberration of the primary (the circle of least confusion of the uncorrected prime focus is about 20 arcmin in diameter) and feeds the corrected prime focus with an f/4.2 beam. The SAC yields a circular, flat, science field of view of 8 arcmin in diameter, with a 1-arcmin annulus around it for guide stars used in closed-loop guiding.

The entrance pupil of the SAC is 11 m in diameter and can thus accept light from celestial targets from the entire primary mirror. However, as the Tracker tracks celestial objects, the alignment of the SAC entrance pupil must necessarily be offset with respect to the primary mirror, so that parts of the primary mirror outside the entrance pupil do not contribute to light reaching the focal plane. Fortunately, the exit pupil of the optical system is readily accessible and a moving hexagonal baffle at this position is kept aligned with the primary mirror, thus preventing stray light from the periphery of the primary mirror reaching the focal plane. The telescope is equipped with an atmospheric dispersion compensator (O'Donoghue 2002) to enable access to wavelengths as short as 320 nm without image-quality degradation arising from atmospheric dispersion.

As mentioned, the axis of symmetry of the primary mirror is tilted with respect to the zenith by 37°, so that the accessible declination range is $+10\overset{\circ}{.}5$ to $-75\overset{\circ}{.}3$. Celestial targets are accessible to the telescope when they enter an annular region which is centred on the zenith and has an angular distance (with respect to the zenith) of 37°. The range of the Tracker is $\pm$ 6° so that a celestial target is accessible when its zenith distance lies in the range 31°–43°. These constraints permit objects to be tracked for a duration of 1 h at the northern end of the accessible declination range, and more than 3 h at the southern end.

The mode of operation of the telescope is straightforward: the telescope is slewed to the appropriate azimuth for a given celestial target. The primary mirror is stationary at this azimuth during the observation. When the desired celestial target enters the annular region of accessibility, it is tracked using the Tracker. Most celestial targets are accessible twice in a given night: once in the eastern sky and once in the western sky. At the extreme north and south ends of the declination range, targets can be re-acquired by re-positioning of the telescope in azimuth, thus permitting more than two pointings.

2 SALTICAM: THE SOUTHERN AFRICAN LARGE TELESCOPE IMAGING CAMERA

Among the First Light instrumentations for the SALT (Buckley et al. 2003, 2004) is an ultraviolet-visible (UV-visible) simple imager, SALTICAM.

Due to the interests of many of the scientists in the consortium partners, capability at the shortest wavelengths accessible from the ground ($\sim$320 nm) and high time-resolution in the detectors are features of the first generation of instrumentations on the telescope. The observations presented in this paper were made with SALTICAM. This instrument has already been described elsewhere (O'Donoghue et al. 2003), but a brief summary is given here to provide context for the data to be discussed below.

SALTICAM was designed to fulfill a number of functions: a camera to provide an instrument for the telescope as early during its commissioning and testing phase as possible; the acquisition camera for the telescope; and a simple imaging instrument with a high time-resolution capability. Its detector comprises a mosaicked pair of E2V Technologies 44–82 CCDs: 2048 × 4102 × 15 μm pixel (60 × 30 mm^2 of imaging area). Each CCD is coated with the E2V Astro Broad Band coating providing excellent UV sensitivity, is made of deep depletion silicon to provide additional sensitivity and less fringing in the I band, and has two low-noise ($\sim$3 electron pixel^{-1}) readout amplifiers. Each CCD has independent vertical clock lines for each half of the chip and can thus be operated in frame-transfer mode.

The f/4.2 focal ratio of the SALT yields a plate scale of 224 μm arcsec^{-1} so that an 8-arcmin field spans 107.5 mm with considerable oversampling of 15 μm pixel. SALTICAM was thus equipped with a seven-element lens system to re-image the 8-arcmin field on the pair of CCDs described above at a scale of 107 μm arcsec^{-1} (and a focal ratio of f/2.0). The lenses are made of UV transmitting crystals: fused silica, BaF_2 and CaF_2 thereby affording excellent transmission for wavelengths as short as 320 nm.

As mentioned, high time-resolution capability was one of the scientific drivers for the instrument, with 0.1-s sampling for point sources identified as a requirement. The large 44–82 CCDs have

considerable on-chip capacitance, necessitating a rather slow vertical clocking rate of 100 μs per row. Vertical clocking of half of each chip in standard frame-transfer operation would thus add ∼0.2 s, thereby ruling out achievement of the requirement. To circumvent this difficulty, 'slot mode' operation was devised. In this mode, a mask with a slot of width projecting to 144 (unbinned) rows (20 arcsec) on the CCDs is positioned just above the frame-transfer boundary of the chips (which are aligned co-linearly with respect to each other). The slot does not lie on the CCDs, of course, but ∼2 mm above, so there is a region of partial vignetting. Only the central 72 rows receive all the light. The slot extends the full 8 arcmin in the horizontal direction. After each exposure, only 144 rows are transferred across the frame-transfer boundary, thereby shortening the vertical clocking overhead to 14 ms. Each image takes a few exposures to 'migrate' to the readout register but this presents no particular problem and allowance is made for this in the time-stamping of the data which is done by hardware interrupts from the South African Astronomical Observatory time service. This time service is accurate to better than 1 ms.

The detectors are housed in an evacuated cryostat, cooled to 160 K by a CryoTiger closed-cycle cooler, and controlled by an SDSU II CCD controller with custom developed software. A standard 100-mm Prontor shutter was modified to use two solenoids for 'flip-flop' opening and closing (to avoid needing a solenoid to be powered up and therefore a potential source of heat for the duration of each exposure). The shutter is, of course, held open during rapid sampling as described in the previous paragraph. Finally, a filter unit allows one of eight exchangeable, broad-band filters to be inserted into the beam under software control for any given exposure.

Further description of the instrument, including quantitative details and more information on the high time-resolution capability, is given in O'Donoghue et al. (2003, 2004).

3 ECLIPSING AM Her STARS (OR POLARS)

Amongst the shortest period binaries known are AM Her stars, also called Polars. A subclass of CVs, they are semidetached binaries in which a Roche lobe-filling lower main-sequence star (usually an M star) transfers mass to a highly magnetized ($\sim 10^7$–$10^{8.5}$ G) white dwarf. The magnetic field of the white dwarf (the primary) inhibits the formation of the standard thin accretion disc found in most CVs and instead channels the gas flowing from the lower main-sequence star (the secondary) to accretion regions at or near the magnetic poles of the white dwarf. About 85 such systems are known with orbital periods ranging from 87 min to ∼8 h (see Schwope et al. 2004 for a review of eclipsing polars, and Wickramasinghe & Ferrario 2000; Warner 1995; Cropper 1990 for more general reviews of AM Her stars).

In the broader context, these systems are valuable laboratories for studying magnetic accretion on to compact objects, found in many other astrophysical scenarios from pulsars to active galactic nuclei.

Usually, the gas falling on to the white dwarf is thermalized in a strong shock at or above the white dwarf surface and may outshine most other sources of radiation in the system, emitting radiation from X-ray to infrared wavelengths. The footprint on the white dwarf where the accretion occurs is also very small: typically 10^{-4} of the surface area of the star.

Eclipsing polars are very valuable examples of these systems as the eclipse of the white dwarf by the secondary allows indirect mapping of the gas flow and accretion on to the white dwarf. High time-resolution is, however, critical as the accretion regions are eclipsed by the secondary in only 1–6 s. SALTICAM's efficiency at all optical wavelengths and high time-resolution makes it highly suitable for studies of eclipsing polars such as SDSS J015543+002807, the topic of this paper. The primary aim is to resolve the eclipse ingress/egresses of the accretion region(s). Similar work on other eclipsing polars using a Superconducting Tunnel Junction detector has been described by Perryman et al. (2001), Bridge et al. (2002) and Reynolds et al. (2005). There is also discussion on unpublished results obtained by ULTRACAM and OPTIMA in Schwope et al. (2004).

4 SDSS J015543+002807

This object was identified in the Sloan Digital Sky Survey as an eclipsing CV (Szkody et al. 2002). Follow-up optical photometry, showing very deep eclipses, has been published by Dubkova, Kudryavtseva & Hirv (2003) and Woudt, Warner & Pretorius (2004).

Wiehahn et al. (2004) (hereafter W2004) confirmed that the star was indeed a polar based on polarimetry which showed variations in circular polarization between −10 and +10 per cent, along with strong linear polarization. The photometry obtained as part of the polarimetric data showed that the system brightness declined very rapidly (in a matter of a few seconds or even less).

During the W2004 observations, the system was in a low-luminosity state. Schmidt et al. (2005) (hereafter S2005) confirmed the polarization, extending the range of measurements to the 'high' brightness state of the system. They also discussed X-ray observations and found that the optical emission lines changed to absorption lines during certain orbital phases. Neither W2004 nor S2005 could decide whether or not there were one or two accreting poles in the system.

Because of the rapid, deep eclipses, implying that the optical emission originates from a compact region on the white dwarf, SDSS J015543+002807 is a highly suitable target for observations with SALTICAM as described below.

5 OBSERVATIONS

During the SALTICAM commissioning observing run, time-series imaging of SDSS J015543+002807 was obtained by the SALT+SALTICAM on the nights of 2005 August 5/6, 6/7, 10/11, 11/12 and 2005 September 6/7 and 7/8. Exposure times ranged between 112 and 285 ms (the time to move each image behind the mask, during which image smearing takes place, is 14 μs). A summary log of the 4.3 h of observations appears in Table 1. Altogether nine time-series were obtained, eight of which included eclipses of the target star: the second sequence on 2005 September 06/07 did not include an eclipse.

The observations were made with the instrument in 'slot mode' as described in Section 2. There were problems in managing the data flow between the SDSU II CCD controller and PC during the August observations, so gaps of about 6 s, while the data were being displayed and written to disc, appear in these data at intervals of typically 18–20 s. These problems had been almost entirely solved by the time of the September data. The instrument maintained strict time using a stable 1-kHz signal originating from a GPS receiver which also provided UTC. The instrument computer stamped the header of each frame with the time of the exposure and this was subsequently used to calculate the Heliocentric Julian Date (HJD) for all frames. We have not used the more uniform Barycentric Julian Dynamical Time as previous timings have not used this system. To convert all timings in this paper to BJDD [JD(TDB)], add 67.12 s to the August data and 67.14 s to the September data.

Table 1. High-speed clear filter photometry and eclipse timings of SDSS J015543+002807. Contact times (all in days) listed in the table refer to the ingress/egress of Spot 1 (first line) and Spot 2 (second line) of the corresponding run. The missing entries arise because the timing was not available, due to gaps in the data. The O−C values (in parentheses) for mid-eclipse timings are in units of 0.000 001 d. See the text for more details.

Date 2005	Exposure time (ms)	Run length (min)	Eclipse cycle	HJD	First contact	Mid ingress	Second contact	Mid eclipse (and O−C)	Third contact	Mid egress	Fourth contact
August											
05/06	285	10.1	10 234	245 3588+					0.648 009	0.648 021	0.648 036
				245 3588+	0.644 692	0.644 705	0.644 715				
06/07	230	12.3	10 250	245 3589+	0.612 659	0.612 670		0.614 473 (−4)	0.616 269	0.616 277	0.616 288
				245 3589+	0.612 930	0.612 943	0.612 954	0.614 474 (−4)	0.615 998	0.616 005	0.616 025
06/07	230	33.4	10 251	245 3589+	0.673 189	0.673 200	0.673 211	0.674 992 (−2)	0.676 780	0.676 785	0.676 795
				245 3589+		0.673 468	0.673 476	0.674 992 (−2)	0.676 504	0.676 517	0.676 533
10/11	230	26.3	10 317	245 3593+	0.667 264	0.667 277	0.667 293	0.669 069 (−3)	0.670 848	0.670 862	0.670 872
				245 3593+	0.667 541	0.667 552	0.667 562				
11/12	230	26.5	10 332	245 3594+	0.575 008	0.575 019	0.575 029				
				245 3594+	0.575 270	0.575 283	0.575 296	0.576 817 (0)	0.578 341	0.578 351	0.578 365
September											
06/07	112	45.4	10 761	245 3620+	0.536 510	0.536 518	0.536 529	0.538 317 (−6)	0.540 104	0.540 115	0.540 126
				245 3620+	0.536 782	0.536 794	0.536 800	0.538 318 (−5)	0.539 837	0.539 843	0.539 863
06/07	112	15.5									
06/07	112	45.9	10 762	245 3620+	0.597 027	0.597 035	0.597 053	0.598 832 (−7)	0.600 602	0.600 630	0.600 638
				245 3620+	0.597 300	0.597 309	0.597 316	0.598 834 (−5)	0.600 353	0.600 360	0.600 376
07/08	112	41.5	10 777	245 3621+	0.504 795	0.504 804	0.504 819	0.506 600 (+15)	0.508 376	0.508 396	0.508 419
				245 3621+	0.505 068	0.505 079	0.505 095	0.506 604 (+19)	0.508 116	0.508 128	0.508 144

Because of the shortness of the exposure times, and the decline of the star to fainter than 20th magnitude at mid-eclipse, the observations were made through a clear filter comprising 5 mm of WG295: the filters in SALTICAM are located in the strongly converging f/2 beam, so having no filter would significantly degrade image quality. *BVR* filtered observations were tried but the loss of light, combined with poor image quality at the time these data were obtained, has rendered them of limited use.

The instrument thus provided a sequence of images 8 arcmin long, but only 20 arcsec wide. These images were split into four distinct sections, corresponding to the four readout amplifiers of the two CCDs. In order to facilitate the shortest possible exposures, 4 × 4 (August) and 6 × 6 (September) prebinning was used. This did not lead to undersampling of the images: each prebinned pixel corresponded to 0.56 (August) and 0.84 (September) arcsec and the combination of seeing and the image quality of the telescope at the time was modest, between 1.5 and 2.0 arcsec (full width at half-maximum).

High-accuracy *absolute* photometry with the SALT is very difficult because of the moving entrance pupil and resulting variable aperture as described in Section 1. Fortunately, all stars within the field of view of the telescope lose the same fraction of light due to mismatch between the pupil and the primary mirror (as well as the small gaps between the primary mirror segments). Provided the brightness of the comparison star(s) is known, the absolute brightness of other stars in the field can be recovered. The data presented here are all referenced to the nearby star, 27 arcsec to the west and 5 arcsec north of the target star; its magnitudes and colours in the Sloan Digital Sky Survey filter set appear in Dubkova et al. (2003). The comparison star and the target star were imaged within the same amplifier.

No flat-field calibration frames were obtained (the calibration system was not available at the time of the observations) and the frames were simply bias-subtracted using overscanned pixels from each row. Despite this, the errors in the photometry are very small (∼0.02 mag outside eclipse). Stellar magnitudes were extracted using standard CCD photometry techniques and the brightness of the target star was referenced to that of the comparison star mentioned above.

6 LIGHT CURVES

Although the August data quality is somewhat affected by the gaps, these and (especially) the September data constitute the highest time-resolution/highest signal-to-noise ratio (S/N) light curves of eclipsing polars of which we are aware. It is thus worth describing them in some detail.

Fig. 1 shows the full data set on an intensity scale (i.e. the intensity is proportional to the brightness of the target), and phased using the orbital ephemeris derived in the next section (see equation 1 below). The light curves show the features already reported by other authors: an asymmetric orbital modulation with a gradual rise to a maximum at orbital phase ∼0.1 followed by a more rapid decline; the eclipse interrupts the light curve just before maximum. During the orbital phase interval 0.90–0.95, there is a pre-eclipse dip of variable shape and depth, which has been attributed to obscuration by the mass-transfer stream of the strong emission originating at the accretion columns/spots on or close to the white dwarf primary. Note that the intensity of each run is on the *same* scale, as the data were referenced to the comparison star mentioned above.

Superimposed on the orbital modulation are stochastic brightness variations typical of CVs. In contrast to the high-frequency flickering in polars, such as VV Pup, for example, the variations in this star occur on a time-scale of minutes rather than seconds. On short time-scales, the light curve is quite smooth.

Fig. 2 shows, in the left-hand and right-hand panels, more detail around the eclipse in both magnitudes and intensity, respectively, as different information is conveyed in each panel. In order to improve the S/N, especially at the bottom of the eclipse, most of the data in Fig. 2 have been averaged: with the exception of the portions during the precipitous brightness changes, where the original

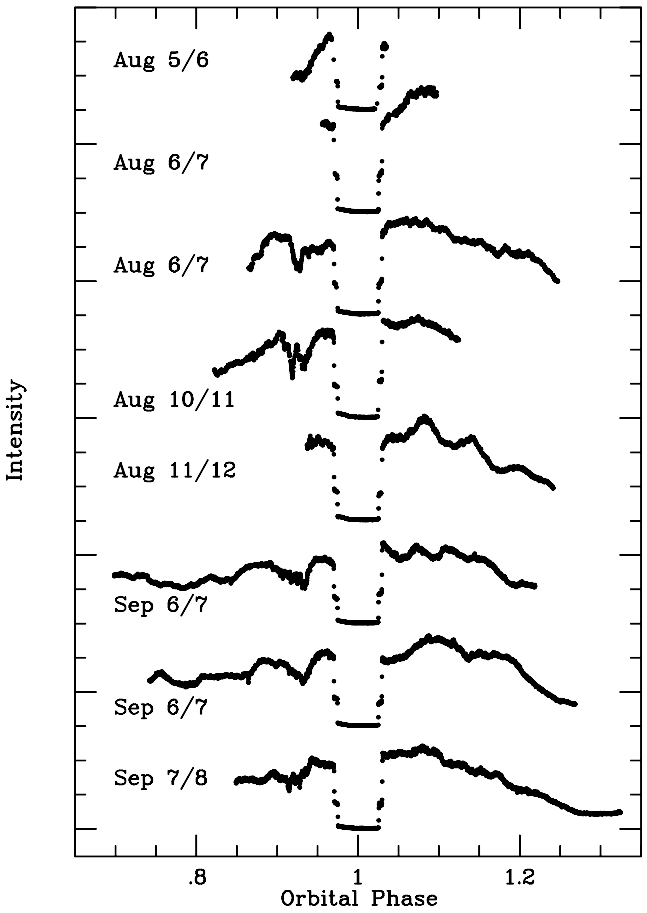

Figure 1. High-speed photometry listed in Table 1 (except for the second section on 2005 September 06/07). The horizontal axis is orbital phase using the ephemeris of equation (1). Its carets (0.05 phase) correspond to ∼260 s. The vertical axis is relative intensity in arbitrary units (i.e. linearly proportional to the brightness of the star). Its zero-point is the lowest caret on the vertical axis. Individual runs have been offset from adjacent runs by three carets on the vertical axis. The points are 1-s averages of the original data.

time-resolution has been retained (Table 1), the points in the plot are 1-s averages of the original data.

The most notable feature of Fig. 2 is the stepped shape of the eclipses, visible in every eclipse (taking into account the missing sections in the August data). At phase ∼0.97, there is a very rapid decline of ∼1.0 mag, followed at phase ∼0.975 by another very rapid decline of ∼2.5 mag. There is then a much more gradual further decline of ∼1.5 mag over a time-interval of ∼105 s up until phase 0.0. In some light curves, the bottom of eclipse is flat; in others there is a slight rise (∼0.5 mag) just before the very rapid increase in brightness at ∼1.026. There is then a plateau similar to that seen on ingress and lasting ∼0.005, followed by the last very rapid emergence occurring at ∼1.030.

The right-hand panels show the same data on an intensity scale which emphasizes different features to the left-hand panel: the first drop/last rise is brighter than the second (contrary to the impression given in the left-hand panel). Also, the fading between phases 0.975 and 1.000 is much less obvious and the light curve from phase 1.000 to 1.030 looks essentially flat. *The two precipitous brightness changes thus account for almost all the flux in these light curves*.

As mentioned already, SDSS J015543+002807 has been established to be a polar (W2004, S2005). Within this context, Figs 1–2 allow some immediate conclusions to be drawn. These are most easily appreciated with the aid of Fig. 7 (left-hand panel). The Roche lobe-filling M dwarf is shown in black to indicate its minimal contribution to the light curve. Its limb has just begun to eclipse the photosphere of the white dwarf. On (or near) the surface of the white dwarf are two bright spots (shown as white in the inset) which give rise to almost all the light from the system and which cause the stepped structure of the eclipse comprising two precipitous brightness changes in a very short time, with a standstill in between. We will refer to these spots as 'Spot 1' and 'Spot 2' as indicated in Fig. 7. We are aware that although we have described the features as located on the surface of the white dwarf, they may, perhaps even more likely, be accretion columns *above* the surface of the white dwarf. In order to avoid clumsy wording, we will simply refer to them as spots, but all the time bearing in mind that they may not be located on the surface of the white dwarf.

The rest of the white dwarf is shown in dark grey: the standstills at orbital phases 0.9725 and 1.0275 are not entirely flat and usually show a small decline/rise on ingress/egress indicating that the white dwarf photosphere, which is being covered/uncovered at these phases (see Fig. 7), does contribute a small amount of light.

While the shading chosen for the components in Fig. 7 is intended to illustrate their relative light contributions, and is somewhat arbitrary, the dimensions are accurately computed from Roche lobe geometry for a specific mass ratio, inclination and white dwarf radius. The location and extent of the spots shown are consistent with producing the observed light curves. The relevant parameters are not unique, of course, and further analysis will be given in Sections 8 and 9. A similar diagram is shown as fig. 4 in Perryman et al. (2001) in their study of the eclipsing polar UZ For which also has a similarly shaped eclipse indicative of two bright regions on the surface of the white dwarf. Other sources of light in that system make a significant contribution, however, so the eclipse is not nearly as deep as in SDSS J015543+002807.

Other aspects of the eclipse light curves shown in Fig. 2 are also interesting: the magnitude scale of the left-hand panel was calculated by assuming that the comparison star has a 'clear filter' magnitude (i.e. weighted over the 600 nm range of sensitivity of the CCDs) of 16.7. We expect that this rough zero-point will be accurate to ∼0.3 mag. The resulting brightness of the target is slightly fainter than 15th mag just before eclipse. It is thus clear that the target was in its bright luminosity state for the duration of the observations presented here (see figs. 2–4 of S2005). With respect to its brightness just before or just after eclipse, the star is ∼5 mag fainter at the faintest part of the eclipse.

In other eclipsing polars (e.g. UZ For: Perryman et al. 2001; HU Aqr: Bridge et al. 2002), there is also a gradual decline in brightness similar to that seen in Fig. 2 between orbital phases 0.975 and 0.0. This is explained as eclipse of emission from the accretion stream as it flows towards the accretion region(s) on or near the white dwarf. Clearly, a similar explanation is warranted here. Presumably, reappearance of parts of the stream accounts for the rounded shape to the bottom of the eclipse as opposed to, say, light contributed by the secondary star. We defer detailed study of the accretion stream to a later paper.

7 ECLIPSE EPHEMERIS

Fig. 3 shows the eclipses of Spots 1 and 2 on an expanded horizontal scale and at the time-resolution of the original data. The ingress/egress of the spots takes place in ∼1–2 s.

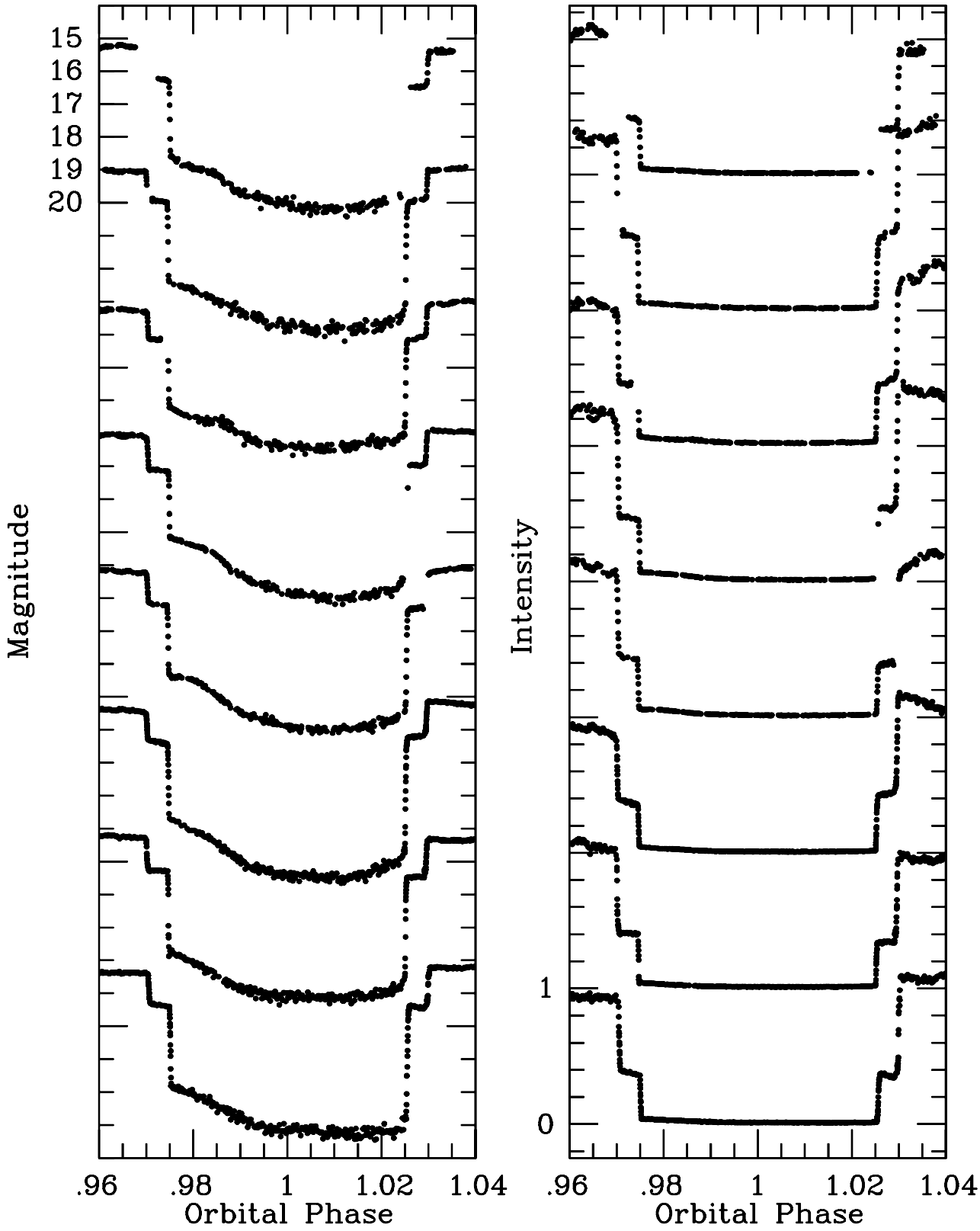

Figure 2. High-speed photometry shown in Fig. 1 around the time of eclipse with the vertical axis in magnitudes (left-hand panel) and intensity (right-hand panel). The ordering of the individual runs is as in Fig. 1. The horizontal axis is orbital phase using the ephemeris of equation (1). Individual carets (0.005 phase) correspond to ∼26 s. The vertical axis of the left-hand panel is in magnitudes and is intended to show detail at the bottom of eclipse. Its overall zero-point is accurate to ∼0.3 mag (the relative zero-point from run to run is known much more accurately). Individual runs in this panel have been offset from adjacent runs by four carets on the vertical axis. The vertical axis of the right-hand panel is intensity as in Fig. 1. The zero level of each run occurs at the large caret marks (i.e. individual runs have been offset from adjacent runs by five carets on the vertical axis). With the exception of the points occurring in the precipitous brightness changes, where the original time-resolution has been retained, the points in both panels are 1-s averages of the original data.

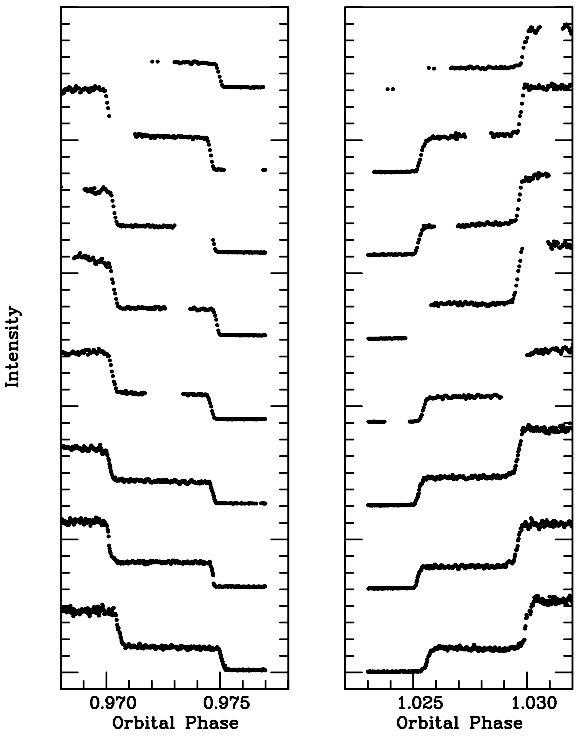

Figure 3. Ingress and egress detail. The ordering of the individual runs is as in Figs 1 and 2. The horizontal axis is orbital phase using the ephemeris of equation (1). Individual carets (0.001 phase) correspond to ∼5.2 s. The vertical axis is relative intensity as for Fig. 1. Its zero-point is indicated by the lowest caret on the vertical axis. Individual runs have been offset from their neighbours by five carets on the vertical axis.

Estimates of the time of first to fourth contact as well as mid-ingress and mid-egress (defined as the time when half the light in the spot is eclipsed) of both spots were made by inspecting large-scale plots and referring to the times of the points on the plot. These times are listed in Table 1, with the values for Spot 1 on the first line and those for Spot 2 on the second line of the entry for that run. We estimate that the 1σ random error of this method is one sampling time (second column of Table 1). It turns out that the time of mid-eclipse (defined as the mean of the times of mid-ingress and mid-egress) of Spot 1 is almost identical to that of Spot 2. Accordingly, a separate timing of mid-eclipse for each spot was made and the results are also listed in Table 1 where the cycle numbers use the zero-point of W2004. These timings were used along with all those listed in S2005 and W2004 to derive a linear ephemeris for mid-eclipse; the residuals with respect to this ephemeris are shown in the top panel in Fig. 4. The large scatter at negative cycle numbers is due to these timings being made from conventional CCD observations on modest-sized telescopes with exposure times of minutes. The fast photometric and polarimetric data of Woudt et al. (2004), W2004 and the present data (cycles −1000 to 11 000) have scatter lower by at least a factor of 10 so these were selected and used to derive the ephemeris for mid-eclipse of both spots shown in equation (1):

$$\mathrm{HJD} = 245\,2969.322\,083 + 0\overset{\mathrm{d}}{.}060\,516\,3312\ \mathrm{E} \qquad (1)$$

$$\text{Mid-eclipse} \qquad \pm 5 \qquad \pm 7$$

The residuals with respect to this ephemeris are plotted in the lower panel of Fig. 4 and listed, for the SALTICAM data, in parentheses in the column in Table 1 labelled 'Mid-eclipse'. The ephemeris is consistent with previous ephemerides (e.g. W2004, S2005), ex-

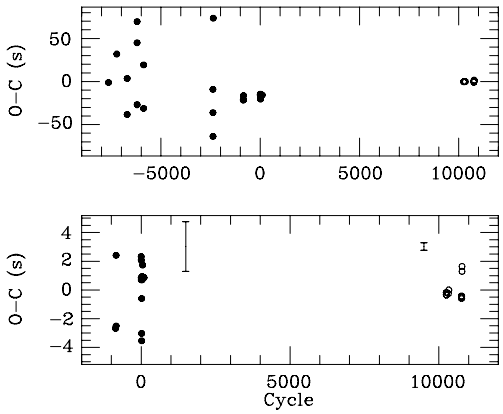

Figure 4. O−C diagram for all available eclipse timings with respect to the ephemeris of equation (1). The top panel shows all available timings including those listed in S2005, except for the two with the largest error bars. The ephemeris was derived from the timings in the lower panel which are the best-quality subsets from the upper panel. The error bar positioned at cycle 9500, O−C 3.0 s in the lower panel shows the 2σ uncertainties for the SALTICAM timings. The error bar positioned at cycle 1500, O−C 3.0 s shows the 2σ uncertainties for the W2004 timings (see their table 2).

tends over a much longer baseline and is of much higher quality. It was used for the conversion from time to orbital phase throughout this paper. Note that the epoch in the ephemeris is *not* necessarily that of conjunction of the two stars; the white dwarf was not detected in our observations.

With the exception of the last SALTICAM run on 2005 September 7/8, the scatter of the SALTICAM residuals is less than 0.5 s (peak to peak) and consistent with measurement error (see the caption to Fig. 5 for an explanation of the measurement error). The timings associated with the last run differ from the ephemeris by more than measurement error: this is obvious from Fig. 3 in which the lowest eclipse shown occurs distinctly later than that in the other runs. Post facto checks of the instrument timings give no reason to doubt the

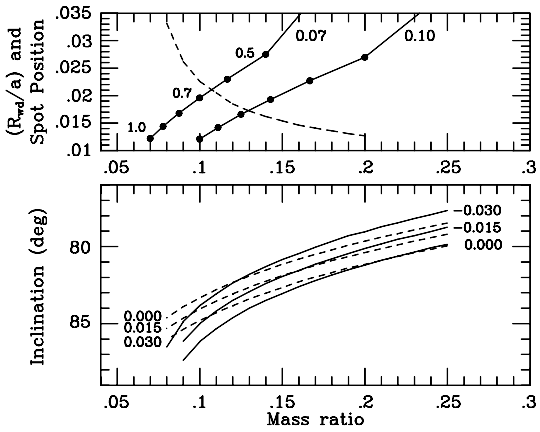

Figure 5. Lower panel: plot of inclination versus mass ratio. The continuous lines with negative numerical labels refer to the displacement of Spot 1 below the orbital plane; the dashed lines with positive numerical labels refer to the displacement of Spot 2 above the orbital plane. See the text for further details. Upper panel: plot of distance of spots with respect to the orbital plane (dashed line) and radius of the white dwarf (continuous lines) versus mass ratio. Labels 0.07 and 0.10 refer to the mass of the secondary, and labels 0.5, 0.7 and 1.0 refer to the mass of the primary. See the text for further details.

accuracy of the timings from the last run. We believe this is a real difference.

The residuals for the times of mid-eclipse of Spots 1 and 2, which are entirely independent measurements, are very similar and also much smaller than the scatter of all the O−C values in Table 1. This not only shows the simultaneity of mid-eclipse for Spots 1 and 2 as previously mentioned, but also shows that there is intrinsic scatter in the times which is larger than measurement error. The former result also confirms the identification of the ingress/egress of Spot 1 as the first/last precipitous brightness change and that of Spot 2 as the second/third precipitous brightness change; further evidence is the similar size of the corresponding brightness changes. The simultaneity of mid-eclipse times of the two spots is remarkable: the largest difference in Table 1 is 0.3 s.

8 BINARY PARAMETERS

The duration of the eclipse of the centre of the primary Roche lobe in a semidetached binary yields a relation between two key parameters: q, the ratio of the mass of the secondary to that of the primary, and i, the inclination of the observer with respect to the binary orbital plane (Horne 1985). In the present situation, things are more complicated.

The standard approach to measuring the duration of eclipse of the centre of the primary Roche lobe is to measure the duration from mid-ingress to mid-egress of the white dwarf primary. This relies on detecting the contact points of eclipse of the white dwarf. Unfortunately, the observed eclipses are dominated by the ingresses and egresses of the two spots. Can the eclipse of the white dwarf nevertheless be detected? An estimate of the relative brightness of the white dwarf can be gauged from the hiatus between the disappearances of the spots on ingress (phases 0.970–0.975 in Fig. 3) or the corresponding feature on egress. At these phases (see Fig. 7), the white dwarf photosphere is being covered/uncovered by the limb of the secondary (it is possible that other sources of light such as the mass-transfer stream close to the white dwarf are also being covered/uncovered). Fig. 3 shows that the light curve is relatively flat in these phase intervals so that the white dwarf photosphere contributes very little light compared to the spots. We attempted to detect the contact points of the white dwarf by looking for changes in slope in the light curve compared to the slope in the phase intervals 0.970–0.975 or 1.025–1.030. We were unable to convince ourselves that these contact points could be identified. We used a light curve synthesis program to simulate eclipses for a wide variety of spot locations and the results lead us to believe that the contact points of the white dwarf must be (almost) coincident with the contact points of the spots. However, it was difficult to explore all possible combinations of parameters so we cannot prove this conjecture.

In the absence of detection of the white dwarf, it is impossible to define the times of eclipse of the centre of the Roche lobe of the white dwarf. The symmetry of the ingresses and egresses of the spots constrains where the spots can lie with respect to each other. More specifically, the very close match between the times of mid-eclipse of both spots shows that the spot locations must lie on the same longitude in this specific reference frame: its origin is at the binary centre of mass; it rotates at the binary orbital period; its x-axis is defined by the line of sight from the earth observer to the binary centre of mass at the time of mid-eclipse of both spots; its x–y plane is tilted to the binary orbital plane by the system inclination. If this were not true, there would be an asymmetry in the timings of the ingresses and egresses of the spots. Longitudes in the reference frame described above correspond to similar but not necessarily precisely equal longitudes in the reference frame of the white dwarf. Such a result is what might be expected if the threading region gives rise to material moving to two spots which are located at the footprints on the white dwarf corresponding to the same magnetic field line, or to two field lines in close proximity.

There is, however, no constraint on the colatitudes of the spots (defined in the conventional manner as the angle between the rotation axis of the white dwarf and the line connecting the centre of the white dwarf and the accretion spot). Either spot might lie at the rotation poles of the white dwarf, or at any colatitude in between, although, as we will now show, there is a constraint on the *difference* of their colatitudes, and even this difference depends on inclination and mass ratio. We can thus only define bounds for the allowable (q, i) combinations.

The approach taken is to define one boundary by estimating the largest reasonable radius for a white dwarf in such a binary, relative to the binary orbital separation, and place the accretion spots at this distance from the centre of the white dwarf above and below the orbital plane. To estimate the largest reasonable relative white dwarf radius, $R_{\rm wd}/a$, the smallest plausible mass white dwarf in a binary with the smallest plausible total mass must be selected. The study of primary and secondary masses in CVs by Smith & Dhillon (1998) suggests minimum masses of 0.07 and 0.5 $\rm M_{\odot}$ for the secondary (M_2) and primary ($M_{\rm wd}$) masses, respectively. The white dwarf models of Wood (1995) along with Kepler's third law yield $R_{\rm wd}$ of 10^9 cm and binary orbital separation, a, of 3.75×10^{10} cm, giving a relative radius for such a white dwarf of $0.027a$. Allowing for an additional 10 per cent if the spots are located above the surface of the white dwarf, we obtain $0.030a$ for the largest relative displacement of the spots above and below the orbital plane.

An eclipse simulation program similar to the kind described in section 2.1 of Horne (1985) to synthesize eclipse light curves of accretion discs was written. This program is functionally the same except that, in this case, eclipse light curves of white dwarfs and their accretion regions were modelled. The number of free parameters was small: the mass ratio and inclination; the brightness of the white dwarf photosphere; the brightness, location and size of the spots. Combinations of q and i were determined which gave eclipses of spots located as described in the previous paragraph and whose ingress/egress occurred at the observed orbital phases of ± 0.0297 (Spot 1) and ± 0.0252 (Spot 2).

The other boundary was defined by determining combinations of q and i which gave eclipses of the centre of the white dwarf between -0.0297 and -0.0252 (i.e. one or other spot is coincident with the centre of the white dwarf projected on the plane of the sky). An intermediate case of spots located at $0.015a$ was also computed. The results are shown in the lower panel of Fig. 5.

The continuous lines with negative numerical labels refer to Spot 1; the dashed lines with positive numerical labels refer to Spot 2. The numerical labels refer to the displacements, in units of a, of the relevant spot with respect to the centre of the white dwarf. Provided that the input assumptions are correct, allowable (q, i) combinations lie somewhere in the locus defined by the intersection of the region bounded by the $-0.03a$ and $0.0a$ continuous lines and the region bounded by the $0.0a$ and $0.03a$ dashed lines. Once a specific value of q and i is fixed, the *difference* in colatitudes between the spots is then also fixed.

Fast photometric observations in the low state of the same kind as presented here will hopefully reveal the contact times of the white dwarf. With this information, the exact values of q and i can be determined from the intersection of the appropriate continuous line for Spot 2 with the appropriate dashed line for Spot 1. For the moment, however, the necessary information is unavailable. Note

that there is a minimum total separation of about $\sim 0.017a$ (at $q \sim 0.25$) for the spots: if the separation is smaller, there is no intersection of the region bounded by the dashed lines with the corresponding region bounded by the continuous lines. At the lowest mass ratios, there is a maximum total separation of about $\sim 0.06a$ (at $q \sim 0.08$).

The upper panel of Fig. 5 enables further conclusions about the allowed range of binary parameters to be drawn. The dashed line in this panel was calculated under the assumption that the two spots are equidistant from the centre of the white dwarf and the binary orbital plane. The locus of allowed (q, i) combinations is no longer a bounded area as in the lower panel, but a curve. This curve maps to the dashed line in the upper panel which shows as a function of q the distance of the spots from the orbital plane in units of a.

To explain the continuous lines in this panel, a consideration of the masses of the component stars is needed. The revised orbital period–secondary mass relation of Smith & Dhillon (1998) predicts $M_2 \sim 0.070\,\mathrm{M}_\odot$ in SDSS J015543+002807 (averaging their linear and power-law fits). Older relationships (e.g. Warner 1995) expect $0.10\,\mathrm{M}_\odot$. The secondary in OY Car, an eclipsing dwarf nova with a very similar orbital period, has a mass of $0.07\,\mathrm{M}_\odot$ and this is likely to be accurate, as the component masses of the system were measured by one of the most-reliable measurement techniques known (Wood et al. 1989). Thus, $0.07\,\mathrm{M}_\odot$ is the best estimate for the mass of the secondary in SDSS J015543+002807.

As far as the primary is concerned, as noted above, a lower limit of $0.5\,\mathrm{M}_\odot$ for the white dwarfs in CVs is apparent in fig. 5 of Smith & Dhillon (1998).

The horizontal coordinate of the continuous lines in the upper panel is based on the mass ratio resulting from, respectively, $M_2 = 0.07$ or $0.10\,\mathrm{M}_\odot$ (large labels at upper right-hand side of each continuous line) combined with $M_{\rm wd}$ ranging from 0.5 to $1.0\,\mathrm{M}_\odot$: the filled circles on the continuous lines show $M_{\rm wd}$ of 0.5, 0.6, 0.7, 0.8, 0.9 and $1.0\,\mathrm{M}_\odot$ with the 0.5, 0.7 and 1.0 points labelled. The vertical coordinate is both the relative distance of the spots above the orbital plane and the ratio of white dwarf radius to orbital separation, with the white dwarf radii taken from Wood (1995).

If the white dwarf mass is such that $R_{\rm wd}/a$ lies *below* the dashed line, at least one of the spots will lie above the white dwarf surface. It is not expected that accretion columns will lie more than, say, $0.1R_{\rm wd}$ above the white dwarf surface, so the plausible range of $M_{\rm wd}$ is 0.5–$0.7\,\mathrm{M}_\odot$ if M_2 has a mass of $0.07\,\mathrm{M}_\odot$, or 0.5–$0.8\,\mathrm{M}_\odot$ if M_2 is $0.1\,\mathrm{M}_\odot$. The same line of reasoning suggests an upper limit of 0.20 or 0.14 for q, again for $M_2 = 0.10$ or $0.07\,\mathrm{M}_\odot$, respectively. Note that even if $R_{\rm wd}$ is larger than the projected spot position, this does *not* imply that the accretion region lies on the photosphere of the white dwarf; it is impossible from the present data to distinguish between this and an accretion column seen projected on the photosphere.

In order to make further progress in the analysis, it is necessary to adopt a specific choice of parameters. We choose $M_2 = 0.070\,\mathrm{M}_\odot, M_1 = 0.60\,\mathrm{M}_\odot$, giving $q = 0.1167, a = 3.96 \times 10^{10}$ cm, and, from Wood (1995), $R_{\rm wd} = 8.9 \times 10^8$ cm $= 0.0225\,a$. We urge that while these parameters are plausible, given the constraints described above, they should be regarded as a *choice* and not a determination, especially as it is likely that further observations will soon lead to much tighter estimates of these parameters.

With the above choices, the light curve synthesis program mentioned previously was used to fix i and locate the spots with respect to the white dwarf. The resulting values were $i = 83.^\circ5$, and colatitudes $\beta = 125^\circ$ and 25° for Spots 1 and 2, respectively (although we must remind the reader that only the difference of the colatitudes is constrained by our data). The longitude of each spot on the white dwarf was chosen to be 0° which is along the line joining the centres of the two stars. The fit of the synthetic light curve to the egress of the second eclipse on 2005 September 6/7 is shown in Fig. 6. We reiterate the previous caution that these parameters are only indicative and not determinations.

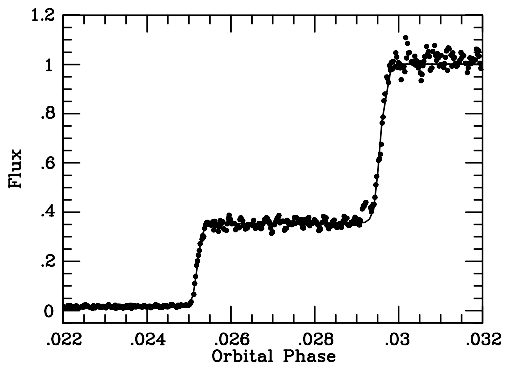

Figure 6. Eclipse egress of the second eclipse from the night of 2005 September 6/7 (points) and synthetic light curve using parameters described in the text (continuous line).

It is worth noting that Perryman et al. (2001), in their analysis of the similar features in the eclipse light curve of UZ For, derived a separation in latitude of the two spots to be in the range 130°–150°. Indeed, they go on to suggest that variations in this separation may be a consequence of variations in the mass-accretion rate.

9 SPOT PROPERTIES FROM DETAILS OF THE ECLIPSES

While the binary parameters cannot yet be fixed, properties of the spots are measurable from the eclipse light curves. Table 2 lists the contact timings of Table 1 with respect to the ephemeris of equation (1). The measurement error indicated, 0.0001 cycles or 0.52 s, is quite conservative, so differences in measurements of the same parameter from eclipse to eclipse of larger than, say, 0.0001 are certainly real. The table shows that the durations of the eclipses of the spots are constant but there is a little jitter in the times when they occur. This suggests that the colatitude of the spots is constant but there are small variations in the longitudes. A convenient way of visualizing some of the information in the table is with the aid of Fig. 7.

The middle panel of Fig. 7 shows the position of eclipse 'diamonds' derived from the contact phases of the eclipses of the spots in all the eight available eclipses. The four sides of the diamonds are defined by the projection of the limb of the secondary star on the plane of the sky at the four contact phases. The intention is to define bounds for the region emitting the light originating from each spot. The filled circle in the middle of the corresponding diamond shows the 'light centre' of each spot, defined as the intersection on the plane of the sky of the projection of the limb of secondary at the phase of mid-ingress and mid-egress of the spot. The right-hand side small panels show the region of the spots in the left-hand panel at a larger scale for clarity.

The dotted lines indicate the relative diameters of white dwarfs with masses of 0.5, 0.6 and $0.7\,\mathrm{M}_\odot$ (assuming $M_2 = 0.070\,\mathrm{M}_\odot$). We reiterate that the white dwarf contact points were *not* detected so its location with respect to the diamonds is only indicative: the centre of the white dwarf could be displaced in longitude or latitude with respect to the spots.

Table 2. Eclipse measurements.

	Date 2005	First contact (cycle) ±0.0001	Mid ingress (cycle) ±0.0001	Second contact (cycle) ±0.0001	Third contact (cycle) ±0.0001	Mid egress (cycle) ±0.0001	Fourth contact (cycle) ±0.0001	Ingress duration (cycle) ±0.0001	Egress duration (cycle) ±0.0001
	August 05/06				0.0296	0.0298	0.0301		0.0004
	August 06/07	−0.0301	−0.0299		0.0296	0.0297	0.0299		0.0003
	August 06/07	−0.0298	−0.0296	−0.0295	0.0295	0.0296	0.0298	0.0004	0.0003
Spot 1	August 10/11	−0.0299	−0.0297	−0.0294	0.0294	0.0296	0.0298	0.0005	0.0004
	August 11/12	−0.0299	−0.0297	−0.0295				0.0004	
	September 06/07	−0.0300	−0.0298	−0.0296	0.0294	0.0296	0.0298	0.0003	0.0004
	September 06/07	−0.0299	−0.0298	−0.0295	0.0291	0.0296	0.0297	0.0004	0.0006
	September 07/08	−0.0296	−0.0294	−0.0292	0.0296	0.0299	0.0303	0.0004	0.0007
	August 05/06	−0.0252	−0.0250	−0.0248				0.0004	
	August 06/07	−0.0256	−0.0254	−0.0252	0.0251	0.0252	0.0256	0.0004	0.0004
	August 06/07		−0.0252	−0.0251	0.0250	0.0252	0.0254		0.0005
Spot 2	August 10/11	−0.0253	−0.0251	−0.0249				0.0004	
	August 11/12	−0.0256	−0.0253	−0.0251	0.0252	0.0253	0.0256	0.0004	0.0004
	September 06/07	−0.0255	−0.0253	−0.0252	0.0250	0.0251	0.0255	0.0003	0.0004
	September 06/07	−0.0254	−0.0253	−0.0252	0.0250	0.0251	0.0254	0.0003	0.0004
	September 07/08	−0.0251	−0.0249	−0.0246	0.0253	0.0255	0.0258	0.0005	0.0005

		Spot 1 Mid-eclipse (cycle) ±0.0001	Spot 2 Mid-eclipse (cycle) ±0.0001	Spot 1 Duration (cycle) ±0.0001	Spot 2 Duration (cycle) ±0.0001	Delta Duration (cycle) ±0.0001
August 05/06						
	August 06/07	−0.0001	−0.0001	0.0298	0.0253	0.0045
	August 06/07	0.0000	0.0000	0.0296	0.0252	0.0044
	August 10/11	0.0000		0.0296		
	August 11/12				0.0253	
	September 06/07	−0.0001	−0.0001	0.0297	0.0252	0.0045
	September 06/07	−0.0001	−0.0001	0.0297	0.0252	0.0045
	September 07/08	0.0003	0.0003	0.0297	0.0252	0.0045

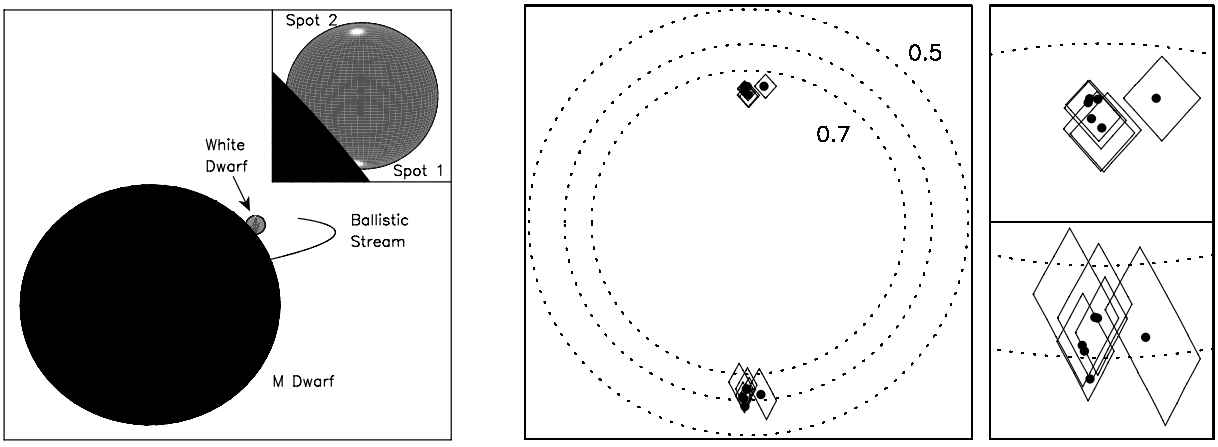

Figure 7. Left-hand panel: view of SDSS J015543+002807 at orbital phase 0.97. The components of the system are labelled. The upper right-hand inset shows the view of the white dwarf at a larger scale. Middle panel: eclipse diamonds defined by the limb of the secondary projected on the plane of the sky at the phases of the four contacts of the eclipses of the spots. The filled circles are the light centres of the spots as defined in the text. The dotted lines show the outlines of white dwarfs with masses of 0.5, 0.6 and 0.7 $M_{\odot}$. The size of the middle panel is 0.058*a* (where *a* is the binary orbital separation). The right-hand panels show the middle panel at larger scale around the diamonds. The size of these panels is 0.008*a*. See the text for more details.

The rightmost upper and lower diamonds originate from the same eclipse, from the night of 2005 September 7/8, whose timing has already been noted to differ from the ephemeris by more than measurement error. With this exception, the other diamonds have considerable overlap with each other. There are, however, changes in size and also in shape, especially in the diamonds in the lower panel which are associated with Spot 1. The projected area of Spot 1 varies between 3.1 and $9.6 \times 10^{-6}\,a^2$, which is between 0.4 and 1.3 per cent that of a 0.5-$M_\odot$ white dwarf, or between 0.8 and 2.4 per cent that of a 0.7-$M_\odot$ white dwarf. This assumes that $M_2 = 0.07\,M_\odot$. The projected area of Spot 2 varies between 2.2 and $4.4 \times 10^{-6}\,a^2$, which is between 0.3 and 0.6 per cent that of a 0.5-$M_\odot$ white dwarf, or between 0.6 and 1.1 per cent that of a 0.7-$M_\odot$ white dwarf. The actual surface area of the white dwarf occupied by these spots will, of course, be larger than this, because we are only measuring the projected area of the spots on the sky, which will be smaller by a factor that depends on the binary parameters, and could be as much as eight times larger for our chosen parameters. A model-dependent conclusion is that the spots subtend at the centre of the white dwarf angles of between 4° and 7°, depending on the mass of the white dwarf. These spot sizes are comparable to those estimated by Cropper & Horne (1994) for ST LMi, although larger regions have been estimated for V347 Pav (Potter, Cropper & Hakala 2000).

As is evident in Fig. 7, the boundaries of the spots and their light centres move around from eclipse to eclipse by typically half the linear size of the diamond. While changes in spot positions have been seen before in polars, particularly associated with accretion-state changes (see e.g. Romero-Colmenero et al. 2003), these are the first data of sufficient quality to see such variations in spot location within an essentially constant accretion state. The diamonds associated with Spot 2 (upper panel) are more tightly distributed, symmetric in shape and smaller in extent than the diamonds associated with Spot 1 which appear elongated along a line of constant longitude. This elongation is not very sensitive to the colatitude of Spot 1. Even when this spot was modelled with a colatitude as extreme as ∼90°, its diamonds were distinctly more elongated than those of Spot 2.

It is also important to emphasize that the diamonds are only boundaries to the accretion spots and only constrain the distribution of enhanced brightness within so as to touch each side of the diamonds. The generally symmetrical shape of the diamonds associated with Spot 2, therefore, does not imply a symmetrical shape for the distribution of light in the spot, which could be more elongated. We defer to a later paper the determination of the surface brightness within the diamonds from the detailed shape of the light curves during ingress/egress of the spots.

10 COMPARISON WITH PREVIOUS OBSERVATIONS AND DISCUSSION

Both W2004 and Woudt et al. (2004) observed the system in its low state. They reported eclipse durations of 312 and 320 s, respectively, which is consistent (given the lower time-resolution and precision of their data) with the duration of the eclipse of Spot 1. In the low state, therefore, this remains the most-luminous spot. In the polarimetry of W2004, positive circular polarization is clearly visible around orbital phase 0.2–0.3. This is consistent with Spot 2 being visible for longer than Spot 1, and positive circular polarization coming from Spot 2 with negative circular polarization coming from Spot 1.

The maximum in the orbital light curve, which occurs *after* the eclipse, is (at least in part) the result of absorption of light which occurs *before* eclipse, presumably in the accretion flow/funnel reported by S2005 (and see below). Two further pieces of evidence favour this interpretation: (i) the appearance of the light curves shown in fig. 15 of Woudt et al. (2004) and in fig. 1 of W2004 which strongly suggests that the bright phase of Spot 1, lasting from orbital phase 0.70 to 1.35, is 'cut into' by absorption; (ii) the centre of the Spot 1 bright phase, $(0.7 + 1.35)/2$, is consistent with Spot 1 closest to the line of sight at mid-eclipse. Consideration must also be given to the contribution of Spot 2 as well as variations caused by cyclotron beaming from both spots.

An additional constraint on the position of Spot 2 might be obtained from noting that our eclipse light curves suggest that all but a few per cent of the optical light arises from the two spots. Around orbital phase 1.3, there is far more optical flux visible (Fig. 1) than a few per cent. Based on this, therefore, Spot 2 never completely disappears from view, requiring that the sum of its colatitude and the system inclination is less than 90°, which in turn suggests that its colatitude is a few degrees or less. This constraint can be 'avoided' if, in the case that Spot 2 does disappear from view, some other light source in the system increases in brightness and compensates for the loss from Spot 2. Heating of the inside face of the M star, or orbital phase dependent variations in the apparent brightness of the accretion flow might behave in this manner. On the other hand, fig. 1 of S2005 suggests that both spots do, in fact, disappear: around orbital phase 0.4, the (hard) X-ray flux falls to zero, or almost zero.

In the low state, there is evidence that Spot 2 is still luminous: the right-hand eclipse in the lower panel of fig. 15 of Woudt et al. (2004), which was obtained with 10-s time-resolution, suggests a hiatus in between the eclipses of Spot 1 and Spot 2. This implies that the overall shape of the eclipse is the same as in our observations so that Spot 2 is still luminous. The significant circular polarization apparent in fig. 1 of W2004 and the substantial (and variable) amount of light visible at orbital phase 0.5 in fig. 15 of Woudt et al. (2004) also support this interpretation. This plot suggests that the relative brightnesses of Spots 1 and 2 are roughly the same as in the high state.

The pre-eclipse dips apparent in Fig. 1 occur from at least orbital phase 0.89–0.96. This is the same range of phases during which S2005 found P Cyg-shaped spectral features which they attribute to absorption by the accretion flow. Their fig. 12 shows that the threading region extends over approximately a factor of 2 in distance from the white dwarf.

The time-resolution of the observations presented here is sufficient to warrant a search for quasi-periodic oscillations. In only one run, ∼10 cycles were seen with a period of about 2 s. However, a single detection made with equipment on a new telescope urges restraint from claiming that the oscillation was intrinsic to the star.

11 SUMMARY AND CONCLUSIONS

The SALT has been completed and first science observations of the polar SDSS J015543+002807 have been obtained. These are high-speed unfiltered photometric observations with time-resolution as short as 112 ms and are the highest-quality observations of this kind of any polar to date. The target was observed in its high-luminosity state and shows rapid eclipses of two compact regions comprising unequivocal evidence for two accretion regions on or near the surface of the white dwarf. These account for all the optical light emitted by the system except for 1.5 per cent at mid-eclipse and

~3–4 per cent from the photosphere of the white dwarf (as distinct from the spots).

The binary system parameters, q and i have been constrained. Further limits, if $M_2 \sim 0.07\,M_\odot$, are $0.5 < M_{wd} < 0.7\,M_\odot, q < 0.14$; or, if $M_2 \sim 0.10\,M_\odot$, are $0.5 < M_{wd} < 0.8\,M_\odot, q < 0.20$. The correlation between i, R_{wd} and the colatitudes of the accretion regions has been explored, and the relative sizes and movements from eclipse to eclipse of the spots have been determined.

In the absence of the detection of the white dwarf, there are few secure constraints on the colatitudes of the spots. The symmetry of the eclipses of each spot suggests that they are located within a small range in longitude.

The dominance of the accretion regions in the luminosity budget of SDSS J015543+002807, combined with its eclipses, offers unusual promise in exploring the details of the accretion regions in a polar. Further observations involving time-resolved spectrophotometry, polarimetry and spectropolarimetry, all of which are available on the SALT, are likely to uncover even more information. This potential can be fully exploited only when high time-resolution observations during the low-luminosity state of the system are obtained. It is likely that the contact points of the white dwarf will then be visible and this information will allow the position of the accretion regions with respect to the white dwarf to be fixed.

ACKNOWLEDGMENTS

We are immensely indebted to the late Dr Bob Stobie. Without his tireless effort and enthusiasm in laying down the foundations of the SALT project at its inception, the observations reported in this paper would never have been made.

We are also immensely indebted to the technical staff of the HET for their generosity in sharing with us which aspects of the design of their telescope were successful and, especially, which were not.

We gratefully acknowledge the shareholders and directors of the SALT Foundation for the usage of the telescope: the National Research Foundation of South Africa; Nicolaus Copernicus Astronomical Centre of the Polish Academy of Sciences; the Hobby–Eberly Telescope Founding Institutions; Rutgers, the State University of New Jersey; Georg-August-Universitat Goettingen; the University of Wisconsin at Madison; Carnegie-Mellon University; the University of Canterbury, New Zealand; the United Kingdom SALT Consortium; the University of North Carolina - Chapel Hill; and Dartmouth College.

We thank an anonymous referee for a very thorough examination of this paper leading to substantial improvements.

REFERENCES

Bridge C. M. et al., 2002, MNRAS, 336, 1129
Buckley D. A. H., Hearnshaw J. B., Nordsieck K. H., O'Donoghue D., 2003, SPIE, 4834, 264
Buckley D. A. H., Cottrell P. L., Nordsieck K. H., O'Donoghue D., Williams T. B., 2004, SPIE, 5492, 60
Cropper M. S., 1990, SSRv, 54, 195
Cropper M., Horne K., 1994, MNRAS, 267, 481
Dubkova D. N., Kudryavtseva N. A., Hirv A., 2003, IBVS, 5389, 1
Horne K., 1985, MNRAS, 213, 129
Meiring J. G., Buckley D. A. H., Lomberg M. C., Stobie R. S., 2003, SPIE, 5489, 592
Meiring J. G., Buckley D. A. H., 2004, SPIE, 4837, 11
O'Donoghue D., 2000, SPIE, 4003, 363
O'Donoghue D., 2002, SPIE, 4411, 79
O'Donoghue D. et al., 2003, SPIE, 4841, 465
O'Donoghue D. et al., 2004, SPIE, 5499, 406
Perryman M. A. C., Cropper M., Ramsay G., Favata F., Peacock A., Rando N., Reynolds A., 2001, MNRAS, 324, 899
Potter S. B., Cropper M., Hakala P. J., 2000, MNRAS, 315, 423
Ramsey L. W., Weedman D. W., 1984, in Ulrich M. H., Kjör K., eds, IAU Coll. 79, Very Large Telescopes, Their Instrumentation and Programs. Armenian Acad. Sci., Yerevan, p. 851
Reynolds A. P., Ramsay G., de Bruijne J. H. J., Perryman M. A. C., Cropper M., Bridge C. M., Peacock A., 2005, A&A, 435, 225
Romero-Colmenero E., Potter S. B., Buckley D. A. H., Barrett P. E., Vrielmann S., 2003, MNRAS, 339, 685
Schmidt G. D. et al., 2005, ApJ, 620, 422 (S2005)
Schwope A. D. et al., 2004, in Vrielmann S., Cropper M., eds, ASP Conf. Ser. Vol. 315, Magnetic Cataclysmic Variables. Astron. Soc. Pac., San Fransisco, p. 92
Smith D. A., Dhillon V. S., 1998, MNRAS, 301, 767
Stobie R. S., Meiring J., Buckley D. A., 2000, SPIE, 4003, 355
Swat A., O'Donoghue D., Swiegers J., Nel L., Buckley D. A. H., 2003, SPIE, 4837, 564
Swiegers J., Gajjar H., 2004, SPIE, 5489, 881
Szkody et al., 2002, AJ, 123, 430
Visvanathan N., Wickramasinghe D. T., 1981, MNRAS, 196, 275
Warner B., 1995, Cambridge Astrophys. Ser. Vol. 28, Cataclysmic Variable Stars. Cambridge Univ. Press, Cambridge
Wickramasinghe D. T., Ferrario L., 2000, PASP, 112, 873
Wiehahn M., Potter S. B., Warner B., Woudt P. A., 2004, MNRAS, 355, 689 (W2004)
Wood M. A., 1995, Lecture Notes in Phys., 443, 41
Wood J. H., Horne K., Berriman G., Wade R. A., 1989, ApJ, 341, 974
Woudt P. A., Warner B., Pretorius M., 2004, MNRAS, 351, 1015

This paper has been typeset from a TEX/LATEX file prepared by the author.